Biomedical Titanium alloy prostheses manufacturing by means of Superplastic and Incremental Forming processes

Antonio Piccininni[1], Francesco Gagliardi[2], Pasquale Guglielmi[1], Luigi De Napoli[2], Giuseppina Ambrogio[2], Donato Sorgente[1], Gianfranco Palumbo[1,a]

[1]*Politecnico di Bari, Department of Mechanics, Mathematics and Management, viale Japigia 182, 70126, Bari, Italy.*
[2]*Università della Calabria, Dipartimento di Meccanica Energia e Gestionale, via Pietro Bucci, 87036, Rende (CS), Italy.*

Abstract. The present work collects some results of the three-years Research Program "BioForming", funded by the Italian Ministry of Education (MIUR) and aimed to investigate the possibility of using flexible sheet forming processes, i.e. Super Plastic Forming (SPF) and Single Point Incremental Forming (SPIF), for the manufacturing of patient-oriented titanium prostheses. The prosthetic implants used as case studies were from the skull; in particular, two different Ti alloys and geometries were considered: one to be produced in Ti-Gr23 by SPF and one to be produced in Ti-Gr2 by SPIF. Numerical simulations implementing material behaviours evaluated by characterization tests were conducted in order to design both the manufacturing processes. Subsequently, experimental tests were carried out implementing numerical results in terms of: (i) gas pressure profile able to determine a constant (and optimal) strain rate during the SPF process; (ii) tool path able to avoid rupture during the SPIF process. Post forming characteristics of the prostheses in terms of thickness distributions were measured and compared to data from simulations for validation purposes. A good correlation between numerical and experimental thickness distributions has been obtained; in addition, the possibility of successfully adopting both the SPF and the SPIF processes for the manufacturing of prostheses has been demonstrated.

1 Introduction

The process of replacing parts of the skeletal system with the adoption of prostheses is not completely optimized, especially in the case of complex bone geometries such as those belonging to the maxillofacial or mandibular regions. One of the most adopted approach is currently based on the reconstruction of a 3D model starting from CT scanning. Through the mirroring technique, it is possible to virtually build the missing part and, thus, to design a prosthetic implant fully customized on the single patient [1]. Despite such process chain is almost completely arranged, the choice of the most suitable material remains still an open question: several examples are well reported in literature as being suitable for biomedical implants. Magnesium and its alloys have been studied over the last century for prosthetic systems thanks to their higher corrosion resistance and biocompatibility [2]. Austenitic stainless steel has been adopted due to its high structural properties and pitting corrosion resistance [3]. Beside metallic materials, bio-ceramics and ceramic coatings have been extensively adopted in the last years [4]: hydroxyapatite is one of the most diffused due to its properties which are very similar to bone's ones, thus promoting the body integration of the implant [5]. Actually, a promising alternative to the above mentioned materials is represented by the adoption of polymers for prosthetic implants: methyl-methacrylate, being cost-effective and reducing the occurrence of intoxication, is widely adopted in cranioplasty [6]. On the other hand, the proper selection of the manufacturing process is a key point: stereolitography, as well as the CAD/CAM approach, is widely adopted since it facilitates, speeds up and improves the quality of surgical procedures [7–10]. Additive manufacturing (3D printing) represents one of the newest process, widely adopted for ABS plastic implants [10,11]. Despite the above described state-of-art, research in such a field is still looking for the best combination of material and process. As concerns the former, lack of structural properties, risks of intoxications or difficulties to obtain complete customized implants make necessary to move the attention towards other materials: Titanium (Ti) alloys are actually considered the best solution, able to match both the aesthetic and the functional requirements to be guaranteed by the implant;

[a] Corresponding author: gianfranco.palumbo@poliba.it

in particular, Ti alloys exhibit low values of the Young's modulus, very similar to that of the cortical bone, thus ensuring a homogeneous stress transfer between the implant and the bone [12,13]; Ti alloys also offer a wide span of properties according to the adopted grades, showing higher ductility and formability from room temperature (commercially pure Ti) up to higher temperature (Ti6Al4V, especially if it is characterised by a controlled microstructure and quantity of alloying elements). In addition, Ti alloys are versatile since they can be easily processed via different manufacturing technologies: (i) powder metallurgy [14], (ii) forming processes [15], (iii) additive techniques [16]. The present work presents some results of the three-years Research Program "BioForming", funded by the Italian Ministry of Education (MIUR) and aimed to investigate the possibility of using flexible sheet metal forming processes, like Super Plastic Forming (SPF) and Single Point Incremental Forming (SPIF), for the manufacturing of Ti alloy prostheses. The prosthetic implants used as case studies in the present work were from the skull; in particular, two different Ti alloys and geometries have been considered: one to be produced by SPF in Ti-Gr23 (or Ti6Al4V-ELI, i.e. the Extra Low Interstitial version of the Ti6Al4V) and one to be produced by SPIF in Ti-Gr2 (i.e. the commercially pure Ti). Numerical simulations, implementing the material behaviours evaluated in the plastic and superplastic field, were preliminary conducted in order to design both the manufacturing processes. Subsequently, experimental tests were carried out implementing numerical results in terms of: (i) gas pressure profile able to determine a constant (and optimal) strain rate during the SPF process; (ii) tool path able to avoid rupture during the SPIF process. Post forming characteristics (thickness distributions) of the prostheses were measured and compared to the correspondent values predicted by simulations for validation purposes.

2 Material and Methods

2.1 Material

In the present work the attention was focused on materials largely preferred as implant materials because of their elastic modulus (similar to the bone's one), low density, non-magnetic properties, low thermal conductivity, high corrosion resistance and good biocompatibility. Ti-Gr2 is considered the most adopted implant material when high mechanical strength is not a priority, since its cost is lower than the Ti6Al4V one [17]. Ti-Gr2 and Ti-Gr23 have been used in this work for manufacturing the prostheses chosen as case studies. The chemical composition of Ti-Gr2 is presented in Table 1.

Table 1. Chemical composition of Ti-Gr2

Fe [%]	C [%]	N [%]	H [%]	O [%]	Ti [%]
0.05	0.00	0.00	0.001	0.13	Bal.

Ti-Gr2 is characterised by good formability at room temperature; for this reason is was chosen for SPIF investigations. SPIF experiments were carried out on 1.5 mm thick square blanks (240 mm x 240 mm) extracted from a commercial sheet purchased in the annealed condition.

SPF experiments were carried out on rectangular blanks (225 mm x 190 mm) extracted from a 1 mm thick Ti-Gr23 sheet. The chemical composition of the sheet, purchased in the annealed condition (790°C for 68 min and then air cooled) is presented in Table 2.

Table 2. Chemical composition of the adopted Ti-Gr23

Al [%]	V [%]	Fe [%]	C [%]	N [%]	H [%]	O [%]	Ti [%]
5.88	3.87	0.14	0.22	0.006	0.002	0.112	Bal.

The material behaviour in the superplastic field was preliminary evaluated by means of an extensive experimental campaign based on free inflation tests: circular blanks extracted from the above mentioned sheet were heated up to 850°C according to literature [18]; free inflation tests were thus conducted setting either a constant gas pressure or several pressure jumps during the same test. Using data from free inflation tests (dome height as a function of the time), material constants (C and m) for defining the *Backofen* power law ($\sigma = C\dot{\varepsilon}^m$) could be evaluated in a strain condition very similar to the one in the real forming process. In particular, material constants to be implemented in the FE model were evaluated both analytically, using the approach proposed by Enikeev and Kruglov [19], and through an inverse analysis based on a genetic algorithm coupled to dome height data from jump pressure tests [20].

2.2 Case studies

One of the main objectives of the present research activity concerns the set-up of a standard procedure that, starting from the damage reconstruction, allows to define the prosthesis profile, also taking into account information about the manufacturing process.

The damage reconstruction was obtained starting from the DICOM image of the skull and implementing a mirroring technique for the skull rebuilding [21]. Great attention was paid to this step of the procedure in order to have the geometry of the prosthesis very similar to the one of the missing anatomical part.

As concerns the implant material, Ti-Gr2 (characterized by high formability at room temperature) was used for manufacturing a prosthesis at room temperature by SPIF, while Ti-Gr23 was used for manufacturing a prosthesis by SPF. Two damage areas were thus considered due to the limitations imposed by the manufacturing process: a frontal prosthesis, to be produced by SPF, and a lateral one, to be produced by SPIF. In Figure 1 the damage areas considered for the prostheses reconstruction have been highlighted.

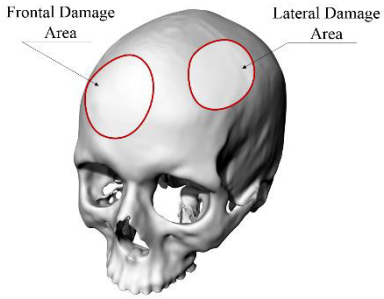

Figure 1. Damage areas.

The lateral prosthesis is shown in Figure 2.a: it is characterized by quite a flat profile and is suitable to be produced at room temperature using the SPIF process. On the contrary, the frontal prosthesis is shown in Figure 2.b: it is characterized by more severe curvature and it can be produced using the SPF process.

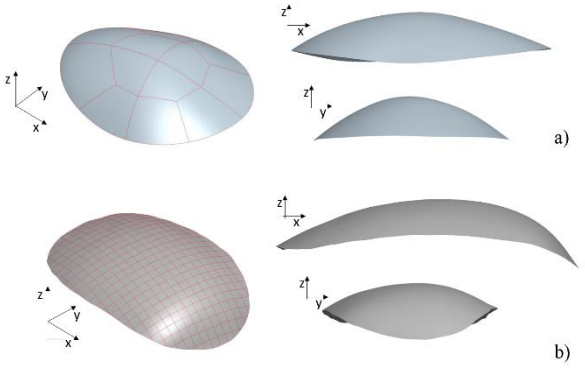

Figure 2. a) Lateral and b) Frontal prostheses.

As concerns the rebuilding of the anatomical part, the steps executed to complete the prosthesis design for both the forming processes have been resumed in Figure 3.

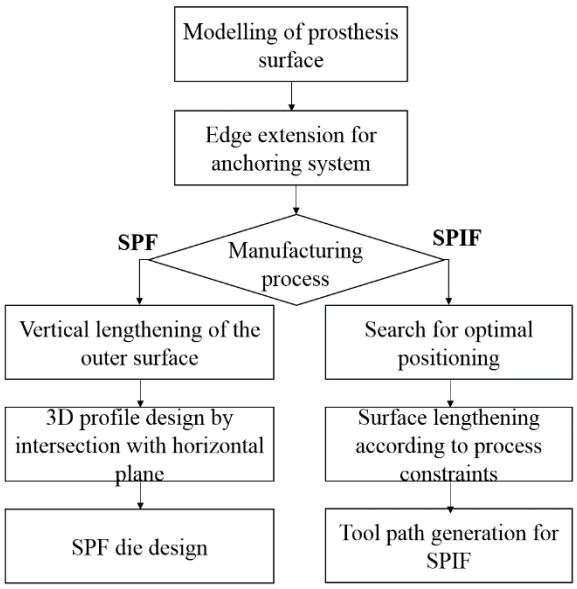

Figure 3. Workflow of adopted procedure

First, the isolated surface was processed to obtain a suitable analytical model. After that, the built surface was extended in order to ensure adequate anchoring of the prosthesis. As a consequence the original periphery of the prosthesis was lengthened in the tangential direction to guarantee the smoothness of the final part. The output of such phase was a larger part suitable to be applied by overlapping on the patient defect and anchored by screws to the skull. In this research an offset of about 13mm was used for both the case studies.

Subsequently the procedure divides into two branches, due to the peculiarity of each forming process: for SPF process the extended periphery was further lengthened in the vertical direction up to the horizontal plane on which the original blank is clamped by the Blank Holder. The sharp angularities at the intersection were smoothed by means of proper fillet radii. The final geometry of the prosthesis for the SPF process is reported in Figure 4.

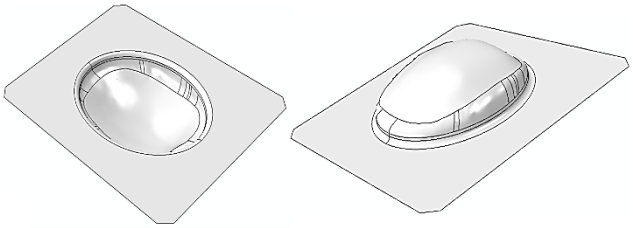

Figure 4. Prosthesis reconstruction for SPF process.

As concerns the SPIF process, the right shape positioning on the sheet plane was performed considering the technological constraints of the SPIF process [22]. More deeply, an optimization loop was carried out to maintain the orientation of the geometry to be SPIFed, with respect to the clamping plane, below the formability limits of the investigated material. Once the clamping plane was set, the analytical surface of the prosthesis was extended up to it, tangentially from the extended periphery. The final geometry of the prosthesis to be produced by the SPIF process is shown in Figure 5.

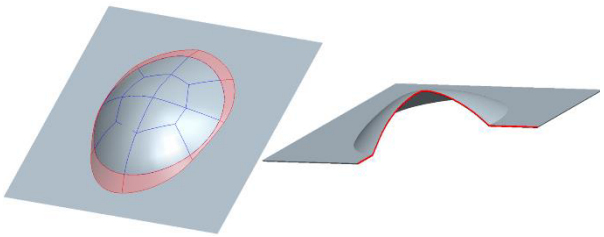

Figure 5. Prosthesis reconstruction for SPIF process.

Finally, the obtained geometries of the prostheses were used to define the die geometry (in the case of the SPF process) and the CAM part program (in the case of the SPIF process).

2.3 Experimental equipment

2.3.1 SPF equipment

SPF tests were carried out using a 2500 kN prototype hybrid electro-hydraulic press machine. The closing force is ensured by four electric motors supported, when

necessary, by two additional hydraulic cylinders. SPF experimental tests were carried out at 850°C adopting heated tools (maximum temperature: 1000°C). As shown in Figure 6, the upper tool was equipped with a 310S die insert in which the geometry of the prosthesis was created by machining.

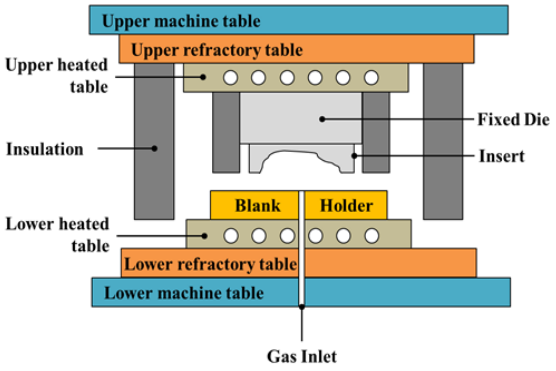

Figure 6. Main component of the press machine for SPF tests.

Tools were heated by means of six electric cartridges (13.2 kW per single tool) managed by a Programmable Logic Control (PLC). Temperature monitoring was provided by K-type thermocouples placed close to both the die and the blankholder surfaces: when a uniform temperature distribution was reached (5°C between the upper and the lower tool) the heating was stopped. Once reached the working temperature, the blank was thus introduced between the tools and then clamped (480 kN); experimental test were carried out setting the same temperature used for characterization purposes (850°C), being this value reported in literature as favourable to emphasize the superplastic properties of the investigated alloy [18]. Before the test, boron nitride was applied on both the surfaces of each blank, in order to make easier the extraction of the formed part. SPF test were carried out implementing optimized pressure laws directly coming from the numerical simulation.

2.3.2 SPIF equipment

Due to its cheapness, the use of the SPIF technology can be strategic in fields like the medical one, since natural differences in terms of anthropometrical items of each individual is a fundamental production constraint. Moreover, SPIF process seems the natural candidate for skull manufacturing since the use of customised dies has to be absolutely rejected [23].

As introduced in the previous section, a part program was generated using a CAD/CAM system. More in detail, the manufacturing module of Pro-Engineering was adopted for generating the tool path. The sheet was positioned on the table of a 3-axes CNC work centre, where both the SPIF step and the trimming one could be executed. An image of the experimental set up is shown in Figure 7.

In addition, a "general purpose" backing plate was positioned under the sheet to support the same during the process. A simple HSS tool having an hemispherical profile with 12mm of diameter was used. After the forming step, the subsequent cutting operation was executed to remove the sheet periphery; in particular, a small milling tool, having a diameter of 5 mm, was adopted.

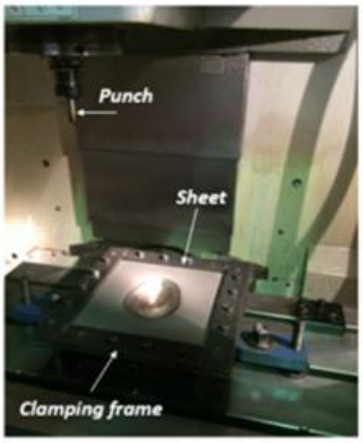

Figure 7. SPIF equipment.

2.4 Numerical model

2.4.1 SPF model

A 3D numerical model shown in Figure 8 was created using the FE commercial code Abaqus.

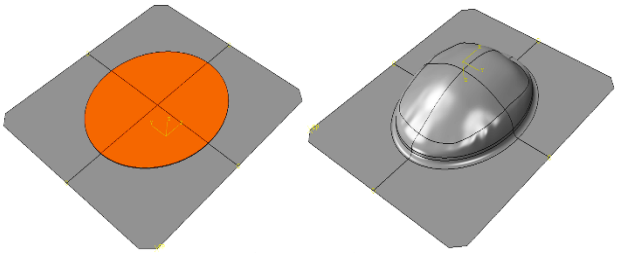

Figure 8. 3D modelling of the die cavity and the Ti blank

Die geometry was modelled through discrete rigid shell elements while the blank as an elliptical deformable body (orange region in Figure 8) meshed using about 8000 linear quadrilateral shell elements (S4R type) with 5 through-thickness integration points, as a good compromise between the accuracy of numerical results and simulation time. In order to correctly simulate the experimental clamping action by the blank holder, the periphery of the blank was pinned. Material superplastic behaviour was modelled according to the *Backofen* power law: in particular, material constants obtained analysing free-inflation tests data using both the analytical approach [19] and the inverse analysis [20] were implemented. Coulomb's friction law was implemented in all simulations, setting the Coefficient of Friction to the value of 0.1.

2.4.2 SPIF model

SPIF numerical simulations were set out by *Hypermesh*, creating the FE model (LS-Dyna) shown in Figure 9.

The sheet (only the region deformed by the punch) was uniformly meshed by quad elements having a side length equal to 4mm; 50 elements were utilized for each sheet side in its initial configuration. In order to take into account the clamping action exerted by the blank holder in the SPIF experiments, the periphery of the modelled blank was pinned.

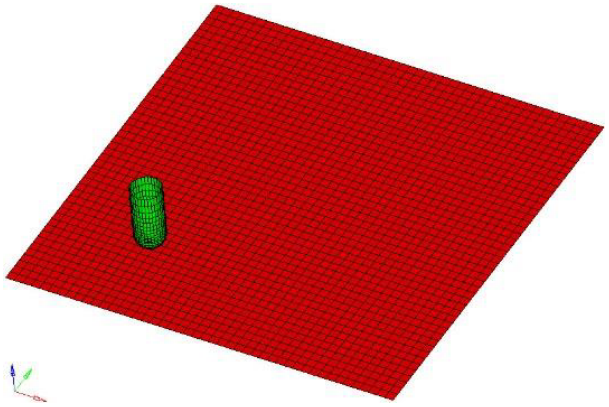

Figure 9. FE model in LS-Dyna.

Blank elements with the Tsay–Hill formulation and five integration points along the thickness were used. An adaptive mesh refinement with four maximum refinements was implemented to adapt the solution accuracy superimposing finer sub-grids in the most deformed regions. The strain rate dependent isotropic plasticity law (MAT-019) was used to consider the plastic deformation of the sheet. The punch, modelled as rigid, was moved according to prescribed boundary curves along the three Cartesian axes. Finally, the contact interface between the punch and the sheet was automatically defined using contact surfaces (Forming-Surface-To-Surface). Coulomb's friction model with a constant value (0.1) was implemented in SPIF simulations. The carried out numerical analysis was based on the explicit formulation: both the time scaling and the mass scaling approaches were utilized, verifying the energy condition of the model during the simulation. In particular, considering the adopted explicit formulation, a check on the total kinetic energy was carried out, verifying that the quota added virtually was lower than the 5 per cent of the internal energy [24]. Finally, with regard to time scaling, the simulation time was about 30 minutes with a time step of 2.5 E-5 s (a dual processor Xeon 3.2GHz with 16 GB RAM was used).

3 Results

3.1 Numerical results

3.1.1 SPF numerical results

Since the investigated alloy exhibited a highly pronounced superplastic behaviour when subjected to a strain rate of 2E-4 s^{-1} at the working temperature of 850°C [18], a pressure profile able to keep such value was numerically determined using the Abaqus built in routine. Gas pressure was varied ranging from a minimum value of 0.01 MPa up to the maximum pressure level of the press machine (3 MPa).

Numerical simulations were run implementing the two sets of material constants: one coming from the analytical model [19] and the other coming from the inverse analysis [20]. In Figure 10 numerical results have been compared in terms of thickness distributions along the longitudinal path of the formed component, being the equivalent time (t*) equal to 0.4 (i.e. 40% of the total cycle time).

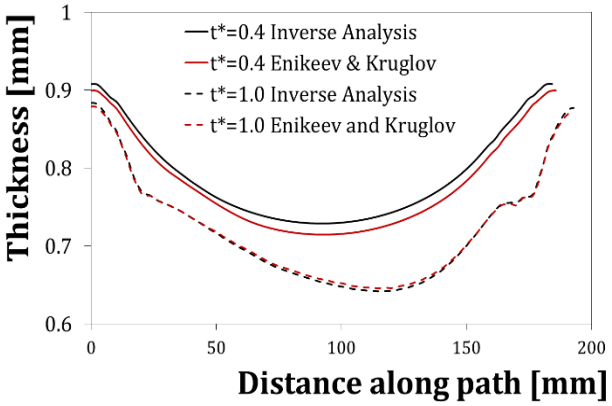

Figure 10. Numerical thickness distributions

It is worthy of notice that the difference between the two distributions is evident. In particular, the simulation implementing the material constants obtained using the analytical approach predicts higher thinning of the part. On the contrary, when t* is equal to 1.0 (i.e. at the end of the SPF process) the two distributions are almost overlapped. In Figure 11 results concerning the same conditions (t* equal to both 0.4 and 1) but in terms of vertical displacements have been compared (the curves have been arranged so that the maximum displacement corresponds to an abscissa equal to 0).

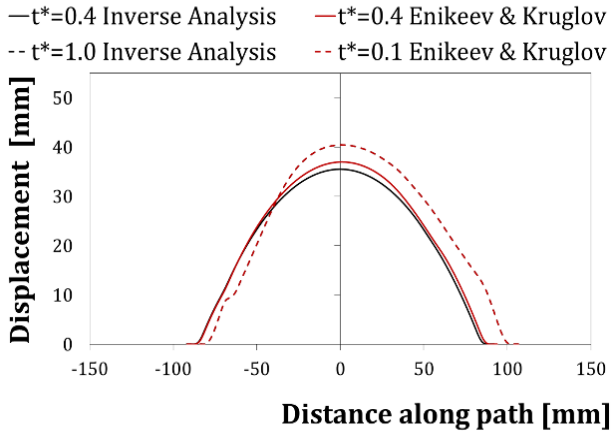

Figure 11. Comparison in terms of vertical displacements

It is worthy of notice that, when the blank (which is deforming under the gas pressure action) touches the die cavity, its profile has to copy the one of the die cavity. For this reason, when t* is equal to 1, the profiles predicted by both models are overlapped.

3.1.2 SPIF numerical results

Each SPIF numerical simulation required about 30min if using a CPU of 3.2GHz and a RAM memory of 16 GB. The final thickness, plotted on the formed sheet, has been reported in Figure 12.

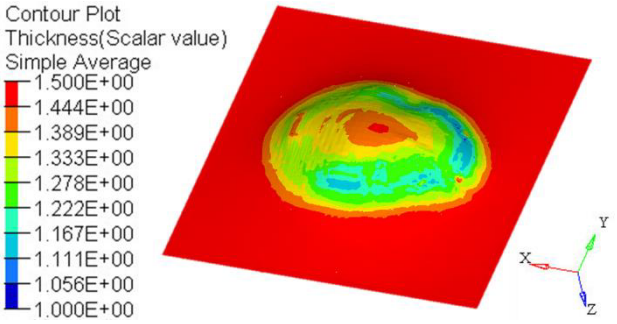

Figure 12. Thickness distribution at the end of SPIF process (mm).

The thickness trend along the symmetry section (x direction) of the prosthesis is furthermore reported in Figure 13.

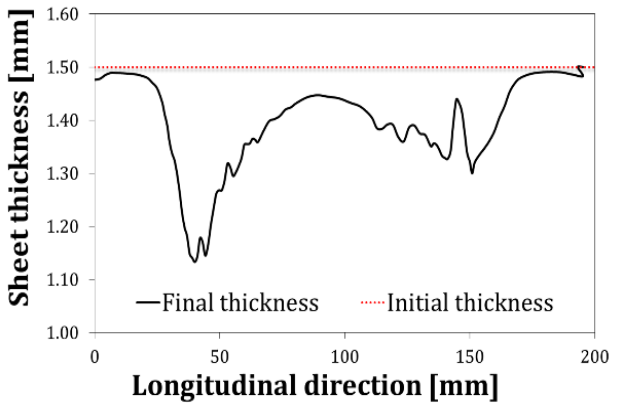

Figure 13. Numerical thickness distribution at the end of the SPIF process

Looking at the results, a minimum thickness of about 1.17mm was reached with a maximum sheet thinning of 22%, which was observed in a small area of the most curved side of the prosthesis.

3.2 Experimental results

3.2.1 SPF experimental results

The final shape of the SPF-ed component was acquired by means of the Digital Image Correlation (DIC) system Aramis. The formed components were painted to create a stochastic pattern able to be recognized by the DIC cameras as a virtual grid (Figure 14. a) DIC cameras, b) acquired shape of the formed component
a).
In such a way it was possible to acquire the final shape of the component (Figure 14. a) DIC cameras, b) acquired shape of the formed component b) and compare the vertical displacement along both the longitudinal and the transversal direction with the correspondent numerical ones.
Formed components were also cut into two halves: in such a way it was possible to measure the thickness distribution along the longitudinal and the transversal direction by means of a calliper.

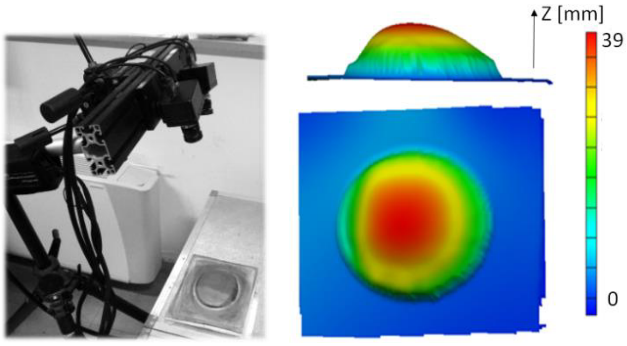

a) b)

Figure 14. a) DIC cameras, b) acquired shape of the formed component

3.2.2 SPIF experimental results

The Ti-Gr2 blank was deformed according to the designed tool trajectory and adopting the following process parameters: a constant tool depth step equal to 0.1 mm and a tool feed rate of about 2000 mm/min. More in detail, the tangential movement of the tool was fully described by the product profile up to obtain the 3D part. The flange region of the SPIFed component was removed and the resulting part has been shown in Figure 15.

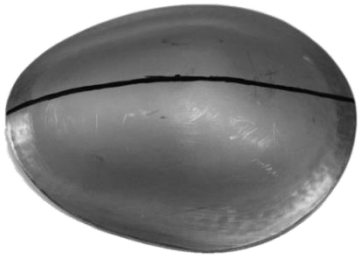

Figure 15. SPIF formed component

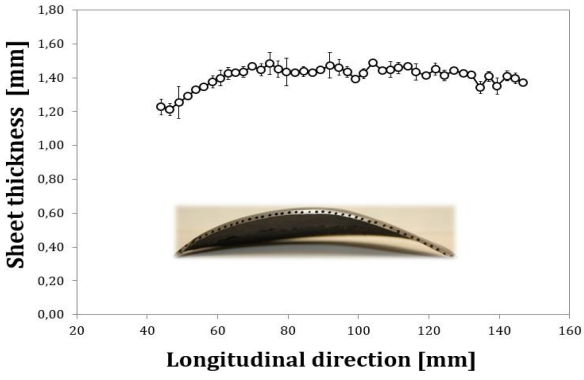

Figure 16. Experimental thickness distribution at the end of the SPIF process

Also in this case the prosthesis was cut into two halves in order to evaluate the thickness distribution: equally spaced points were measured by calliper along the longitudinal direction of the prosthesis. The experimentally measured thickness evolution along the longitudinal direction is reported in Figure 16.

As can be observed, even if a maximum thinning of 0.29 mm was measured at the periphery of the prosthesis (where the effect of the cutting phase is more important) the thickness reduction is less than 1% for the investigated profile.

4 Discussion

4.1 Comparison between experimental and numerical results

Numerical results were compared to the experimental measurements collected in terms of thickness distributions for both the prostheses.

4.1.1 SPF numerical vs experimental

In Figure 17 the numerical thickness distribution has been plotted together with the correspondent experimental one.

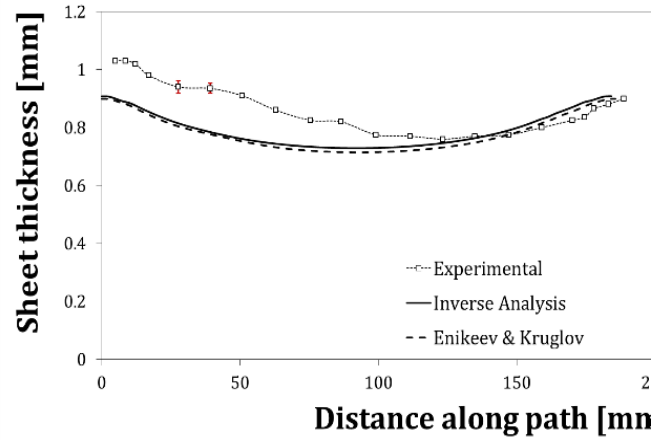

Figure 17. Numerical vs. experimental thickness distribution (t^*=0.4)

It is important to put in evidence that a better agreement was found when implementing the material constants coming from the inverse analysis (with respect to the one implementing the ones obtained using the analytical approach by *Enikeev and Kruglov*). This is particularly evident when the parameter t^* is set to 0.4.

At the end of the simulation, the numerical thickness distributions according to the two above mentioned approaches gave the same results, as also confirmed in the bar chart proposed in Figure 18.

In Figure 19 simulation results and experimental data (at the end of the SPF process) in terms of vertical displacements have been compared (like in Figure 11 the curves have been arranged so that the maximum displacement corresponds to an abscissa equal to 0).

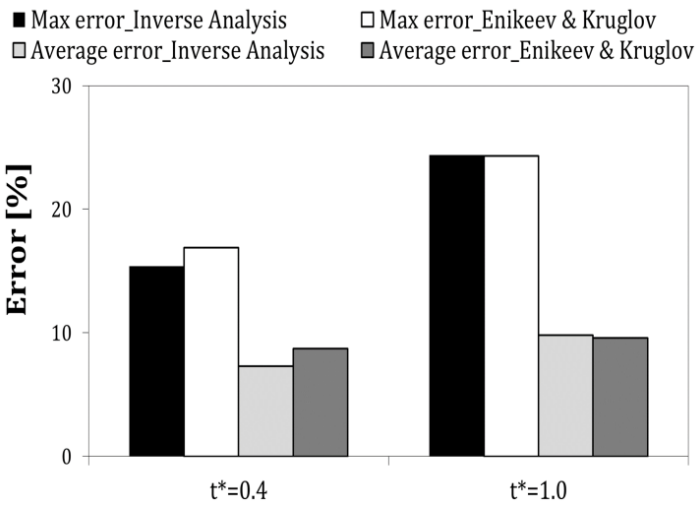

Figure 18. Resume of the comparison between numerical and experimental results.

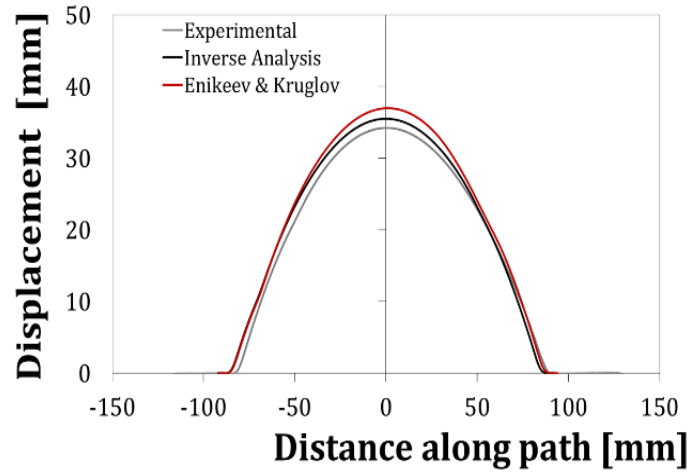

Figure 19. Shape of the formed component: numerical vs. experimental results at t^*=0.4

Such a comparison once again proves the accuracy of the numerical model and the robustness of the approach adopted for the evaluation of the material constants. In fact, as for the thickness distribution, the numerically evaluated shape of the SPF-ed component is closer to the experimental one when implementing in the FE model the material constants obtained from the inverse analysis.

4.1.2 SPIF numerical vs experimental

In Figure 20 the thickness distribution measured on the SPIF-ed component along the longitudinal direction has been compared with the correspondent numerical one.
It is worthy of notice that a suitable overlapping between the numerical and experimental measurements was obtained in the region of the prostheses (external parts where measurements are not present concern the portion of the blank which was trimmed).

Maximum and average prediction errors of about 8% and 4% respectively could be obtained.

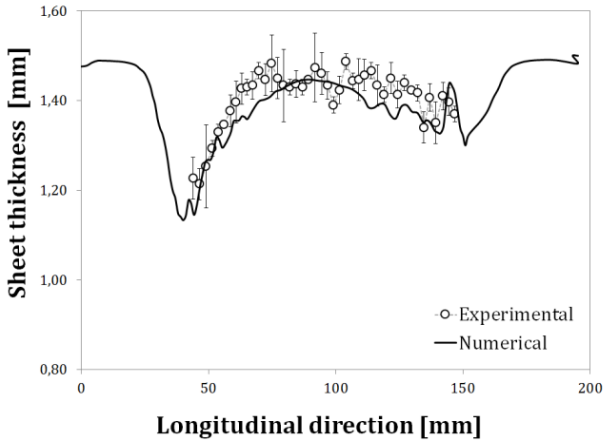

Figure 20. Numerical vs. experimental thickness distribution for SPIF process.

5 Conclusions

Both the materials investigated in the present work, largely preferred as implant materials because of their properties (elastic modulus very similar to the bone's one, low density, non-magnetic properties, low thermal conductivity, high corrosion resistance and good biocompatibility) have confirmed to be suitable for producing prostheses either by Super Plastic Forming (Ti-Gr23) and by Single Point Incremental Forming (Ti-Gr2).

The procedure created in the present research program for producing the prosthesis revealed to be valid: both the die for Super Plastic Forming process and the tool path for Single Point Incremental Forming were obtained.

Finite Element models created for simulating both the forming processes revealed to be robust and accurate, since a good correlation between numerical and experimental thickness distributions could be obtained.

Finally, the possibility of successfully adopting both the Super Plastic Forming and the Single Point Incremental Forming for the manufacturing of Titanium medical prostheses has been demonstrated.

Acknowledgements

The activities in the present work were funded by the Italian Ministry of Education, Universities and Research through the PRIN Project 2012 (project acronym: BIOFORMING).

References

1. S. Katsumura, K. Sato, T. Ikawa, K. Yamamura, E. Ando, Y. Shigeta, et al., Leg. Med. 18 (2016) 37–43.
2. M.P. Staiger, A.M. Pietak, J. Huadmai, G. Dias, Biomaterials. 27 (2006) 1728–1734.
3. S.V. Muley, A.N. Vidvans, G.P. Chaudhari, S. Udainiya, An assessment of ultra fine grained 316L stainless steel for implant applications, Acta Biomater. 30 (2015) 408–19.
4. B.J. McEntire, B.S. Bal, M.N. Rahaman, J. Chevalier, J. Eur. Ceram. Soc. 35 (2015) 4327–4369.
5. G. Staffa, a. Nataloni, C. Compagnone, F. Servadei, 149 (2007) 161–170.
6. J. Jaberi, K. Gambrell, P. Tiwana, C. Madden, R. Finn, J. Oral Maxillofac. Surg. 71 (2013) e81–e88.
7. F.P.W. Melchels, J. Feijen, D.W. Grijpma, Biomaterials. 31 (2010) 6121–30.
8. P. Kasprzak, G. Tomaszewski, G. Wróbel-Wiśniewska, M. Zawirski, Clin. Neurol. Neurosurg. 113 (2011) 311–315.
9. W.-M. Xi, A.-M. Wang, Q. Wu, C.-H. Liu, J.-F. Zhu, F.-F. Xia, Med. Eng. Phys. 37 (2015) 911–915.
10. H.H. Malik, A.R.J. Darwood, S. Shaunak, P. Kulatilake, A.A. El-Hilly, O. Mulki, et al., J. Surg. Res. 199 (2015) 512–522.
11. J. Cohen, S. A. Reyes, Am. J. Otolaryngol. 36 (2015) 1–6.
12. H.J. Rack, J.I. Qazi, Mater. Sci. Eng. C. 26 (2006) 1269–1277.
13. M. Niinomi, J. Mech. Behav. Biomed. Mater. 1 (2008) 30–42.
14. L. Bolzoni, E.M. Ruiz-Navas, E. Gordo, Mater. Sci. Eng. C. 49 (2015) 400–407.
15. F.X. Tan, M.Z. Li, Z.Y. Cai, J. Mater. Process. Technol. 187-188 (2007) 453–457.
16. A.L. Jardini, M.A. Larosa, R. Maciel Filho, C.A. de C. Zavaglia, L.F. Bernardes, C.S. Lambert, et al., J. Craniomaxillofac. Surg. 42 (2014) 1877–84.
17. D. Teker, F. Muhaffel, M. Menekse, N.G. Karaguler, M. Baydogan, H. Cimenoglu, Mater. Sci. Eng. C. 48 (2015) 579–585.
18. H.S. Lee, J.H. Yoon, C.H. Park, Y.G. Ko, D.H. Shin, C.S. Lee, J. Mater. Process. Technol. 187–188 (2007), 526–529.
19. F.U. Enikeev, A.A. Kruglov, Int. J. Mech. Sci. 37 (1995) 473–483.
20. D. Sorgente, A. Piccininni, V. Piglionico, P. Guglielmi, D. Grossi, G. Palumbo, et al., Mater Sci. Forum 839 (2016) 177–182.
21. F. Chen, G.M. Brown, M. Song, Opt. Eng. 39 (2000) 10–22.
22. G. Ambrogio, L. De Napoli, L. Filice, F. Gagliardi, M. Muzzupappa, J. Mater. Process. Technol. 162-163 (2005) 156–162.
23. G. Ambrogio, R. Conte, L. De Napoli, G. Fragomeni, F. Gagliardi, , Key Eng. Mater. 651-653 (2015) 925–931.
24. J. Hallquist, LS-Dyna theory manual, 2001 (STC, Livermore, CA).